Archive of Applied Mechanics (2024) 94:1379–1396
https://doi.org/10.1007/s00419-024-02583-9

ORIGINAL

Shahala Sheikh · Lalsingh Khalsa · Gulshan Makkad · Vinod Varghese

Fractional dual-phase-lag hygrothermoelastic model for a sphere subjected to heat-moisture load

Received: 30 September 2023 / Accepted: 11 March 2024 / Published online: 2 April 2024

Abstract This paper proposes a non-Fourier model of heat and a non-Fick model of moisture diffusion coupling in unification with hygrothermoelasticity theory within the framework of time-fractional calculus theory. The generalized two-temperature theory of hygrothermoelasticity has been used to develop the relevant linearly coupled partial differential equations system. In the context of time-fractional calculus theory, we investigate a hygrothermal elastic problem for a centrally symmetric sphere exposed to physical heat and moisture load at its surface within the limited spherical region. The integral transform approach produces analytical formulas for the transient response of temperature change, moisture distribution, displacement, and stress components in the sphere for pulsed and continuous heat-moisture flux at the sphere's surface. The Gaver–Stehfest procedure is used to invert the analytical hygrothermal variation solutions that were derived in the Laplace domain. The Kuznetsov convergence criterion has studied the problem's stability and bounded variations. The effects of fractional order on the hygrothermal fields and hygrothermoelastic stress response are graphically represented and calculated using numerical data. The specific heat and moisture connection, which abides by Fourier heat conduction and Fick's moisture diffusion, is recovered as a particular case when the fractional-order derivative reduces to the first-order derivative. The study reveals a significant coupling effect between temperature and moisture in composite material T300/5208, with a maximum discrepancy of up to 50%.

Keywords Hygrothermoelastic · Dual-phase lag · Integral transform approach · Fractional calculus · Numerical results

List of symbols

T	Temperature
C	Concentration of water vapor
ϖ, ω	Material constants
C	Mass of moisture
V	Volume fraction of the voids

S. Sheikh · L. Khalsa · G. Makkad (✉) · V. Varghese
Department of Mathematics, M.G. College, Armori, Gadchiroli, India
e-mail: gmakkad@gmail.com

S. Sheikh
e-mail: shahalaimran@gmail.com

L. Khalsa
e-mail: lalsinghkhalsa@yahoo.com

V. Varghese
e-mail: vino7997@gmail.com

ρ_{m}	Density of the material
∇	Gradient operator
Φ	Thermodynamic temperature
b	Discrepancy factor
q_θ	Sectional heat flux
q_ψ	Moisture flux
u_{r}	Radial displacement
E	Young's modulus
υ	Poisson ratio
σ_{rr}	Radial stress
$\sigma_{\theta\theta}$	Tangential stress
$\delta(t)$	Dirac delta function
q_{m}	Moisture flux vector
q_{h}	Heat flux vector
γ	Heat released from a unit mass
C_{p}	Specific heat
k_{h}	Thermal conductivity
k_{m}	Moisture diffusion coefficient
τ_{h}	Relaxation time of heat flux
τ_{m}	Relaxation time of moisture
τ_{q}	Heat flux vector
τ_{T}	Temperature gradient
γ_1	Thermal expansion coefficient
γ_2	Moisture expansion coefficient
s	Transformed parameter
θ	Thermodynamic temperature
φ	Conductive temperature
ψ	Moisture distribution
V	Heat propagation velocity

1 Introduction

The combined effects of temperature and moisture directly influence various materials and structures, such as polymers, porous composites, geomaterials, and asphalt concrete. Numerous researchers have developed different models to simulate how polymers and the composites they form react to the loadings of moisture and temperature. Sih et al. [1] could quantitatively compute the hygrothermal stresses in composite materials using the coupled theory of heat and humidity. The transient responses of an endlessly long hollow cylinder and a solid cylinder that were subjected to hygrothermal loadings were solved by Chang et al. [2] using a linear theory of coupled heat and moisture. Benkhedda et al. [3] established a makeshift model to analyze the hygrothermoelastic stresses in composite laminated plates during desorption without computing the moisture content. Zenkour [4] also presented an analytical explanation for the hygrothermal reactions that occurred in inhomogeneous piezoelectric hollow cylinders when these cylinders were subjected to mechanical and electrical loads. Chiba and Sugano [5] dealt with the one-dimensional transient heat and moisture diffusion and obtained a hygrothermal stress field in a layered plate subjected to hygrothermal loadings. Ishihara et al. [6] investigated the hygrothermal field in a porous media subjected to heat and moisture while considering the nonlinear coupling.

Most of the previously discussed research is founded on the conventional laws of Fourier and Fick, which are widely used to describe heat and mass transfer in many different real-world scenarios. The traditional rules of Fourier and Fick, which have been shown above, do not, however, appropriately reflect a variety of other circumstances. For example, Mitra et al. [7] conducted an experimental investigation to show that the hyperbolic heat conduction model is more suitable in biological materials and can better represent the complete heat conduction process. Tzou [8] explored the lagging behavior for heat transfer in small-scale and quick transitory systems. In the overview study that Hetnarski and Ignaczak [9] wrote about the modeling of thermoelastic waves, they discussed several different models, some of which were the Lord and Shulman model [10], the Green and Lindsay model [11], the Hetnarski and Ignaczak model [12], the Green and Naghdi model [13], and the Chandrasekharaiah and Tzou model [14, 15].

Fractional-order calculus has recently been used in a number of scientific fields, including chemistry, physics, rheology, robotics, engineering, geology, bioengineering, and others, as a logical extension of conventional differential and integral calculus. Fractal polymers, glasses, dielectrics, and semiconductors, to name a few examples, are examples of complex systems that have been the subject of extensive research into fractional-order differential equations as a valuable method to characterize anomalous diffusion [16]. This research has shown that fractional-order differential equations can be a method that accurately describes anomalous diffusion. Depending on the value of the fractional order [17], the time-fractional diffusion-wave equation can classify anomalous diffusion into four groups: subdiffusion, normal diffusion, super-diffusion, and ballistic diffusion. The mathematical properties of the time-fractional diffusion-wave equation are discussed in references [18, 19], which interpolates the wave equation with the parabolic, classical Fourier heat conduction equation.

Recently, Chaves [20] developed a generalized version of Fick's rule, yielding the Levy distribution regarding space-fractional derivatives. Zanette [21] modified the usual Fick's equations to apply to circumstances involving fractional diffusion in which either the waiting time distribution or the displacement probability density showed power-law dropping. Gorenflo et al. [22] were successful in deriving a temporal fractional diffusion equation by employing a fractional Fick's law, which is the rule that governs transport processes that have extended memory. Povstenko [23] utilized the time-fractional diffusion equation to explain the radial diffusion in a sphere of the Dirichlet problem and the Neumann issue, respectively. Later, Povstenko [24] proposed a quasi-static uncoupled thermoelasticity theory based on the heat conduction equation with a time-fractional order similar to the fractional Fick's law.

Sherief et al. [25] and Youssef [26] proposed new thermoelasticity and generalized thermoelasticity theories based on fractional calculus with one relaxation time technique. Ezzat and El-Karamany [27] presented a fresh approach to investigate heat conduction. They used Jumarie [28] fractional Taylor's series to do so. The study conducted by Povstenko [29] focused on the topic of time-fractional thermoelasticity for a sphere under the influence of heat flow. Finally, the authors referred to a few thermoelastic papers that give insight into techniques used in two-temperature thermoelasticity theory [57–60].

Andarwa and Tabrizi [30] studied the coupling of heat and mass transfer with a non-Fourier effect, and Silva et al. [31] presented an extension of the linear Luikov system equations of the coupled heat and transferred through porous media based on a generalization of the Fourier and Fick's laws connected to non-Markovian processes. After conducting additional research, a closed-form solution to the time-fractional hygrothermoelasticity problem for a cylinder with a certain surface temperature and amount of moisture was discovered [32]. In the setting of hyperbolic heat-moisture coupling with varied phase lags of heat and moisture fluxes, Peng et al. [33] examined transient hygrothermoelastic responses in an elastic cylinder subjected to abrupt temperature and moisture change by looking at the behavior of the material.

The present study presents a theoretical framework based on a two-temperature dual-phase-lag time-fractional hygrothermoelastic model to elucidate the influence of coupled heat and moisture on elastic stresses in a centrally symmetric sphere subjected to heat and moisture flux. The linearly coupled partial differential equations for the hygrothermal field have been framed on the two-temperature theory proposed by Sherief et al. [25] and Youssef [26]. It is noted that classical Fourier and Fick's forms have a significant law in assuming an infinitely fast propagation. The Fourier and Fick model has been improved by introducing a given characteristic time constant, known as phase lag of the heat-moisture flux and the temperature-humidity gradient, to remove the paradox of infinite speed propagation. The integral transform approach derivates closed-form solutions of temperature and moisture distribution components over various fractional orders. The numerical Laplace inversion is obtained by using the Gaver–Stehfest algorithm. The non-dimensional numerical values of the results are computed and presented graphically. The proposed dual-phase-lag (DPL) two-temperature model can be reduced to other previously reported models in certain limited cases.

2 Statement of the problem

2.1 Dual-phase-lag hygrothermoelastic theory

Hartranft [34] proposed that the temperature, T, and the concentration of water vapor present in the unit volume of the void, C, are linearly linked to the quantity of moisture absorbed by the solid per unit mass, as $M = \text{constant} + \varpi C - \omega T$, where $\partial M/\partial C = \varpi$ and $\partial M/\partial T = -\omega$. Then, the amount of moisture in

composite per unit mass of solid, m, can be expressed as $\rho_{\mathrm{m}}\, m = VC + \rho_{\mathrm{m}} M$. Due to the presence of liquid and vapor, the moisture and heat transfer obey the conservation of mass and energy as

$$\nabla \cdot q_{\mathrm{h}} = \rho_{\mathrm{m}} \gamma \frac{\partial M}{\partial t} - \rho_{\mathrm{m}} C_p \frac{\partial T}{\partial t} \tag{1}$$

$$\nabla \cdot q_m = -\frac{\rho_m}{V} \frac{\partial M}{\partial t} - \frac{\partial C}{\partial t} \tag{2}$$

Within the framework of the hygrothermal coupling, q_{h} obeys the Fourier law [54, 55] and q_{m} follows Fick's law [39]

$$q_{\mathrm{h}} + \tau_{qh} \frac{\partial q_{\mathrm{h}}}{\partial t} = -k_{\mathrm{h}} \nabla T \tag{3}$$

$$q_{\mathrm{m}} + \tau_{\mathrm{qm}} \frac{\partial q_{\mathrm{m}}}{\partial t} = -k_{\mathrm{m}} \nabla C \tag{4}$$

To examine the microstructural interactions within solid heat conductors at a microscopic level, Tzou [14] presented a dual-phase-lag (DPL) model with delay time translation of the heat flux vector τ_{qh} and temperature gradient τ_{Th} as

$$q(t + \tau_{qh}) = -k_{\mathrm{h}} \nabla T(t + \tau_{Th}),\ k_{\mathrm{h}} > 0 \tag{5}$$

and it is assumed that moisture Fick's law, and presented as a dual-phase-lag model with delay time translation of the heat flux vector τ_{qm} and temperature gradient τ_{Cm}

$$q(t + \tau_{qm}) = -k_{\mathrm{m}} \nabla C(t + \tau_{Cm}),\ k_{\mathrm{m}} > 0 \tag{6}$$

Expanding Eqs. (5) and (6) using fractional Taylor's series of time-fractional order [28] and retaining terms up to the desired order (α,β) in phase lag [56] yields the following result

$$\left[1 + \frac{\tau_{qh}^{\alpha}}{\alpha!} \frac{\partial^{\alpha}}{\partial t^{\alpha}} + \frac{\tau_{qh}^{2\alpha}}{(2\alpha)!} \frac{\partial^{2\alpha}}{\partial t^{2\alpha}}\right] q_{\mathrm{h}} = -k_{\mathrm{h}} \left[1 + \frac{\tau_{Th}^{\alpha}}{\alpha!} \frac{\partial^{\alpha}}{\partial t^{\alpha}} + \frac{\tau_{Th}^{2\alpha}}{(2\alpha)!} \frac{\partial^{2\alpha}}{\partial t^{2\alpha}}\right] \nabla T \tag{7}$$

$$\left[1 + \frac{\tau_{qm}^{\beta}}{\beta!} \frac{\partial^{\beta}}{\partial t^{\beta}} + \frac{\tau_{qm}^{2\beta}}{(2\beta)!} \frac{\partial^{2\beta}}{\partial t^{2\beta}}\right] q_{\mathrm{m}} = -k_{\mathrm{m}} \left[1 + \frac{\tau_{Cm}^{\beta}}{\beta!} \frac{\partial^{\beta}}{\partial t^{\beta}} + \frac{\tau_{Cm}^{2\beta}}{(2\beta)!} \frac{\partial^{2\beta}}{\partial t^{2\beta}}\right] \nabla C \tag{8}$$

in which α and β are the fractional orders, and are limited to lie in a range between 0 and 1. Further, Ignaczak and Ostoja-Starzewski [35, pp. 16–18] analyzed the dual-phase-lag model for integer time derivatives. Here, partial differential equations with fractional derivatives interpolate between elliptic and parabolic equations and between parabolic and hyperbolic equations. In the case of partial differential equations of the fractional order, there is no classification of elliptic, parabolic, and hyperbolic equations. Hence, as mentioned earlier, the statement is widened for partial differential equations of the fractional order and concludes that Eqs. (7) and (8) can be reduced to second-order hyperbolic partial differential equations, if $\tau_{0\mathrm{h}} = \tau_{qh} - \tau_{Th} > 0$, $\tau_{0\mathrm{m}} = \tau_{qm} - \tau_{Cm} > 0$; parabolic if $\tau_{0\mathrm{h}} = \tau_{qh} - \tau_{Th} = 0$, $\tau_{0\mathrm{m}} = \tau_{qm} - \tau_{Cm} = 0$; and elliptic if $\tau_{0\mathrm{h}} = \tau_{qh} - \tau_{Th} < 0$, $\tau_{0\mathrm{m}} = \tau_{qm} - \tau_{Cm} < 0$.

Now, eliminating variables q_{h} and q_{m} in Eqs. (1)–(8), one obtains

$$L\left[1 + \frac{\tau_{qh}^{\alpha}}{\alpha!} \frac{\partial^{\alpha}}{\partial t^{\alpha}} + \frac{\tau_{qh}^{2\alpha}}{(2\alpha)!} \frac{\partial^{2\alpha}}{\partial t^{2\alpha}}\right] \nabla^2 T = \left[1 + \frac{\tau_{Th}^{\alpha}}{\alpha!} \frac{\partial^{\alpha}}{\partial t^{\alpha}} + \frac{\tau_{Th}^{2\alpha}}{(2\alpha)!} \frac{\partial^{2\alpha}}{\partial t^{2\alpha}}\right] \left(\frac{\partial T}{\partial t} - \eta_c \frac{\partial C}{\partial t}\right) \tag{9}$$

$$D\left[1 + \frac{\tau_{qm}^{\beta}}{\beta!} \frac{\partial^{\beta}}{\partial t^{\beta}} + \frac{\tau_{qm}^{2\beta}}{(2\beta)!} \frac{\partial^{2\beta}}{\partial t^{2\beta}}\right] \nabla^2 C = \left[1 + \frac{\tau_{Cm}^{\beta}}{\beta!} \frac{\partial^{\beta}}{\partial t^{\beta}} + \frac{\tau_{Cm}^{2\beta}}{(2\beta)!} \frac{\partial^{2\beta}}{\partial t^{2\beta}}\right] \left(\frac{\partial C}{\partial t} - \lambda_c \frac{\partial T}{\partial t}\right) \tag{10}$$

in which

$$L = k_{\mathrm{h}}/\rho_{\mathrm{m}}(C_{\mathrm{p}} + \gamma\omega),\ \eta_{\mathrm{c}} = \gamma\varpi/(C_{\mathrm{p}} + \gamma\omega) \tag{11}$$

$$D = k_{\mathrm{m}} V/(V + \rho_{\mathrm{m}}\varpi),\ \lambda_c = \rho_{\mathrm{m}}\omega/(V + \rho_{\mathrm{m}}\varpi) \tag{12}$$

If we couple Eq. (5) with the energy equation [36] given by

$$-\nabla q(t) = c\,[\partial T(t)/\partial t],\ c > 0 \tag{13}$$

then there are sequences of the components of a point spectrum that are always such that the real part of the resulting equation approaches infinity. This result demonstrates the problem's instability and indicates that the model is ill-posed and unstable. As a result, even though a constitutive equation intuitively supports our expectations, its mathematical implications force us to reject it. Therefore, based on the findings of Quintanilla [36], it is feasible to hypothesize that the fractional dual-phase-lag model, as depicted in Eq. (9), can be considered stable and well-posed within the framework of the two-temperature hygrothermoelastic theory.

In such a scenario, Chen and Gurtin [37] proposed separating real materials into simple and non-simple categories by considering two temperatures, conductive and thermodynamic, and the two temperatures are related by

$$\Phi = (1 - b\,\nabla^2)\,T,\ b > 0 \tag{14}$$

The thermodynamics and conductivity temperatures exhibit disparities between simple and non-simple materials, although they remain similar for simple materials. In non-simple materials, the thermodynamic quantities depend on the conductive temperature and its spatial derivatives, making these two temperatures no longer equal. The internal energy, entropy, heat flux, and thermodynamic temperature depend on the conductive temperature and its first two spatial gradients. Here, the material parameter b is a crucial distinction between the two-temperature and classical theories. As a limiting case, $b \to 0, \Phi \to T$ give rise to the classical theory.

Now, multiplying $(1 - b\,\nabla^2)$ to both sides of Eq. (9) and neglecting differential coefficients of order higher than ∇^2, one obtains

$$L\left[1 + \frac{\tau_{qh}^{\alpha}}{\alpha!}\frac{\partial^{\alpha}}{\partial t^{\alpha}} + \frac{\tau_{qh}^{2\alpha}}{(2\alpha)!}\frac{\partial^{2\alpha}}{\partial t^{2\alpha}}\right]\nabla^2 T = \left[1 + \frac{\tau_{Th}^{\alpha}}{\alpha!}\frac{\partial^{\alpha}}{\partial t^{\alpha}} + \frac{\tau_{Th}^{2\alpha}}{(2\alpha)!}\frac{\partial^{2\alpha}}{\partial t^{2\alpha}}\right]\left(\frac{\partial \Phi}{\partial t} - \eta_c\frac{\partial C}{\partial t}\right) \tag{15}$$

Thus, Eqs. (10) and (15) express the linearly coupled partial differential equations system the authors are curious about.

2.2 Limiting cases for other model approaches

Applying the various values of phase lags $\tau_{qh},\ \tau_{Th}, \tau_{Cm},\ \tau_{qm}$, one will obtain the following particular cases of hygrothermoelasticity theory as follows:

(i) Taking $\alpha = \beta = 1, \tau_{qh} = \tau_{Th} = \tau_{Cm} = \tau_{qm} = 0$, $b = 0$, and $T = \Phi$ in Eqs. (10) and (15), the model is parabolic and leads to the classical hygrothermal coupled theory (CHTE) [38]

$$L\nabla^2 T - \partial T/\partial t + \eta_c\,(\partial C/\partial t) = 0 \tag{16}$$

$$D\nabla^2 C - \partial C/\partial t + \lambda_c(\partial T/\partial t) = 0. \tag{17}$$

(ii) Taking $\alpha = \beta = 1,\ \tau_{qh} = \tau_{qm} = 0,\ \tau_{Th} \equiv \tau_{0h} > 0,\ \tau_{Cm} \equiv \tau_{0m} > 0,\ \tau_{Th}^2 \to 0\ \tau_{Cm}^2 \to 0$, $T = \Phi$, and $b = 0$ in Eqs. (10) and (15), then the model is hyperbolic and leads to a generalized theory of hygrothermoelasticity [10, 39] given as

$$L\nabla^2 T - [1 + \tau_{0\mathrm{h}}\,(\partial/\partial t)](\partial T/\partial t - \eta_c\,\partial C/\partial t) = 0 \tag{18}$$

$$D\nabla^2 C - [1 + \tau_{0\mathrm{m}}\,(\partial/\partial t)](\partial C/\partial t - \lambda_c\partial T/\partial t) = 0. \tag{19}$$

(iii) Taking $\alpha \in (0,\ 1],\ \beta \in (0,\ 1],\ \tau_{Th} = \tau_{Cm} = 0,\ \tau_{qh} \equiv \tau_{0h},\ \tau_{qm} \equiv \tau_{0m},\ \tau_{qh}^2 \to 0\ \tau_{qm}^2 \to 0, T \neq \Phi$, and $b = 0$ in Eqs. (10) and (15), then the governing equations [40] are identified as work derived for the thermoelasticity formula as a DPL coupled model with a two-temperature hygrothermal model (MHTE)

$$L\nabla^2 T - [1 + (\tau_{0\mathrm{h}}^{\alpha}/\alpha!)(\partial^{\alpha}/\partial t^{\alpha})](\partial T/\partial t - \eta_c\,\partial C/\partial t) = 0 \tag{20}$$

$$D\nabla^2 C - [1 + (\tau_{0\mathrm{m}}^{\beta}/\beta!)(\partial^{\beta}/\partial t^{\beta})](\partial C/\partial t - \lambda_c\partial T/\partial t) = 0. \tag{21}$$

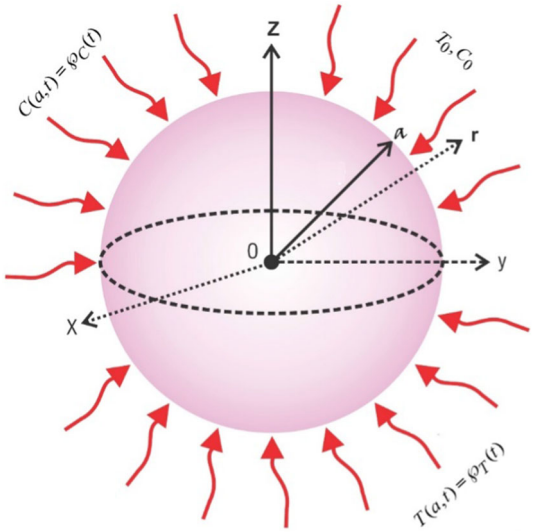

Fig. 1 Schematic of a sphere in a heat, moisture environment

2.3 Hygrothermal field

Consider a perfectly hygrothermoelastic solid sphere with a central symmetry in a homogeneous isotropic thermoelastic medium whose outer surfaces are traction free.

The hygrothermoelastic interactions within the solid sphere are assumed to be spherically symmetric. In this instance, we believe that the hygrothermal influence on elastic stresses and deformation; however, temperature and moisture do not alter as a response to the elastic field. A solid sphere is assumed to occupy the domain $0 < r \leq r_0$, as shown in Fig. 1. Initially, the sphere is kept at a constant temperature and humidity surrounding it, and no external forces are applied through the medium. The following non-dimensional values have been provided as a means of converting the dimensionless system of governing equations:

$$\begin{aligned}\bar{r} =& r/r_0, \theta = (T - T_0)/T_0,\ \psi = (C - C_0)/\lambda_c T_0,\ K = (D/r_0^2)(r_0^2/L)^{\beta/\alpha},\\ \bar{u} =& \zeta u, \vartheta = \Phi/T_0,\ (\bar{t}, \bar{t}^{\alpha}, \bar{\tau}^{\alpha}_{qh},\ \bar{\tau}^{\alpha}_{Th},\ \bar{\tau}^{\beta}_{qm},\ \bar{\tau}^{\beta}_{Cm}) = L(t,\ t^{\alpha}, \tau^{\alpha}_{qh},\ \tau^{\alpha}_{Th},\ \tau^{\beta}_{qm},\ \tau^{\beta}_{Cm})/r_0^2 \end{aligned} \tag{22}$$

The dimensionless form of the governing equations of the model, which has been simplified by dropping the overbar sign for the sake of simplicity, is given as

$$\vartheta = \left[1 - b\left(\frac{\partial^2}{\partial r^2} + \frac{2}{r}\frac{\partial}{\partial r}\right)\right]\theta \tag{23}$$

$$\left[1 + \frac{\tau^{\alpha}_{qh}}{\alpha!}\frac{\partial^{\alpha}}{\partial t^{\alpha}} + \frac{\tau^{2\alpha}_{qh}}{(2\alpha)!}\frac{\partial^{2\alpha}}{\partial t^{2\alpha}}\right]\nabla^2\theta = \left[\frac{\partial}{\partial t} + \frac{\tau^{\alpha}_{Th}}{\alpha!}\frac{\partial^{\alpha+1}}{\partial t^{\alpha+1}} + \frac{\tau^{2\alpha}_{Th}}{(2\alpha)!}\frac{\partial^{2\alpha+1}}{\partial t^{2\alpha+1}}\right](\vartheta - \eta_c\lambda_c\psi) \tag{24}$$

$$\left[1 + \frac{\tau^{\beta}_{qm}}{\beta!}\frac{\partial^{\beta}}{\partial t^{\beta}} + \frac{\tau^{2\beta}_{qm}}{(2\beta)!}\frac{\partial^{2\beta}}{\partial t^{2\beta}}\right]\nabla^2\psi = \left[\frac{\partial}{\partial t} + \frac{\tau^{\beta}_{Cm}}{\beta!}\frac{\partial^{\beta+1}}{\partial t^{\beta+1}} + \frac{\tau^{2\beta}_{Cm}}{(2\beta)!}\frac{\partial^{2\beta+1}}{\partial t^{2\beta+1}}\right]\left(\frac{\psi - \theta}{K}\right) \tag{25}$$

$$\nabla^2 = \frac{\partial^2}{\partial r^2} + \frac{2}{r}\frac{\partial}{\partial r} \tag{26}$$

We look at a physical boundary condition at the surface with the specified initial and boundary values of the matter flux, which is written as

$$\theta(r,0) = \psi(r,0) = 0,\ \frac{\partial\theta}{\partial t}(r,0) = \frac{\partial\psi}{\partial t}(r,0) = 0 \tag{27}$$

$$\theta(1,t) = \wp_{\theta}(t),\ \psi(1,t) = \wp_{\psi}(t) \tag{28}$$

where $\wp_{\theta}$ and $\wp_{\psi}$ are the prescribed sectional heat and moisture flux supply at $r = 1$.

2.4 Hygrothermoelastic field

The equilibrium equation without body force in a spherical coordinate system [41]

$$\frac{\mathrm{d}\sigma_{\mathrm{rr}}}{\mathrm{d}r}+\frac{2}{r}(\sigma_{\mathrm{rr}}-\sigma_{\varphi\varphi})=0 \tag{29}$$

and the stress components in terms of the displacement component u_r are

$$\sigma_{\mathrm{rr}}=\frac{E}{(1+\upsilon)(1-2\upsilon)}\left[(1-\upsilon)\frac{\mathrm{d}u_{\mathrm{r}}}{\mathrm{d}r}+2\upsilon\frac{u_{\mathrm{r}}}{r}-(1+\upsilon)g\right] \tag{30}$$

$$\sigma_{\varphi\varphi}=\sigma_{\phi\phi}=\frac{E}{(1+\upsilon)(1-2\upsilon)}\left[\upsilon\frac{\mathrm{d}u_{\mathrm{r}}}{\mathrm{d}r}+\frac{u_{\mathrm{r}}}{\mathrm{r}}-(1+\upsilon)g\right] \tag{31}$$

where $g=\gamma_1(T-T_0)+\gamma_2(C-C_0)$.

Here, we take for the strain components as $e_{\mathrm{rr}}=\partial u_{\mathrm{r}}/\partial r$ and $e_{\varphi\varphi}=e_{\phi\phi}=u_{\mathrm{r}}/r$; the cubical dilatation e reduces to $e=e_{\mathrm{rr}}+e_{\varphi\varphi}+e_{\phi\phi}=(1/r)[\partial(u_{\mathrm{r}}r^2)/\partial r]$, and the stress–strain equations will take the following forms [41]

$$\begin{aligned}
u_r=&\frac{1}{(1-\upsilon)}\left[(1+\upsilon)\frac{1}{r^2}\int_0^r gr^2\mathrm{d}r+2(1-2\upsilon)\frac{r}{r_0^3}\int_0^{r_0} gr^2\mathrm{d}r\right],\\
\sigma_{rr}=&\frac{E}{(1-\upsilon)}\left[\frac{2}{r_0^3}\int_0^{r_0} gr^2\mathrm{d}r-\frac{2}{r^3}\int_0^r gr^2\mathrm{d}r\right],\\
\sigma_{\varphi\varphi}=&\frac{E}{(1-\upsilon)}\left[\frac{2}{r_0^3}\int_0^{r_0} gr^2\mathrm{d}r+\frac{1}{r^3}\int_0^r gr^2\mathrm{d}r-g\right]
\end{aligned} \tag{32}$$

To convert the dimensionless system of governing equations, we introduce the following non-dimensional quantities as

$$\overline{\sigma}_{\mathrm{rr}}=\frac{(1-\upsilon)\sigma_{\mathrm{rr}}}{E\gamma_1T_0},\ \overline{\sigma}_{\varphi\varphi}=\frac{(1-\upsilon)\sigma_{\varphi\varphi}}{E\gamma_1T_0},\ \overline{u}_{\mathrm{r}}=\frac{u_{\mathrm{r}}(1-\upsilon)}{\gamma_1(1+\upsilon)T_0r_0} \tag{33}$$

If we assume that the dimensionless displacements, strains, and stresses are the functions of r, t only, then the equation of motion in terms of the displacement u without external body forces is given by

$$\begin{aligned}
\overline{u}_{\mathrm{r}}=&\frac{1}{\overline{r}^2}\int_0^{\overline{r}}\overline{g}\,\overline{r}^2\mathrm{d}\overline{r}+\frac{2(1-2\upsilon)}{1+\upsilon}\,\overline{r}\int_0^1\overline{g}\,\overline{r}^2\mathrm{d}\overline{r},\\
\overline{\sigma}_{\mathrm{rr}}=&2\int_0^1\overline{g}\,\overline{r}^2\mathrm{d}\overline{r}-\frac{2}{\overline{r}^3}\int_0^{\overline{r}}\overline{g}\,\overline{r}^2\mathrm{d}\overline{r},\\
\overline{\sigma}_{\varphi\varphi}=&2\int_0^1\overline{g}\,\overline{r}^2\mathrm{d}\overline{r}+\frac{1}{\overline{r}^3}\int_0^{\overline{r}}\overline{g}\,\overline{r}^2\mathrm{d}\overline{r}-\overline{g}
\end{aligned} \tag{34}$$

where $\overline{g}=\theta+(\gamma_2/\gamma_1)\lambda_c\psi$, and the primes, as shown in Eq. (34), will no longer be included as we proceed. Further, it is assumed that the sphere experiences no external forces or restrictions on its outer surface, that is, traction free at $\sigma_{\mathrm{rr}}(1,\,t)=0$. Moreover, considering the quiescent state, the initial values of displacement u_{r} and the stresses σ_{rr}, $\sigma_{\varphi\varphi}$, and their first-order time-derivative, are uniformly zero. When a mechanical stimulus is applied, the classical solution can be hired to calculate the corresponding elastic reactions. These individual replies can be overlaid to generate the complete set of elastic responses. Therefore, the present study focuses on the flexible reaction to hygrothermal loading.

3 Solution of the problem

3.1 Solution of the heat conduction problem

Applying Laplace transform to Eqs. (23)–(25) and using Eq. (27), we get

$$\vartheta^* = \left[1 - b\left(\frac{\partial^2}{\partial r^2} + \frac{2}{r}\frac{\partial}{\partial r}\right)\right]\theta^* \tag{35}$$

$$\left[1 + s^{\alpha}\frac{\tau_{qh}^{\alpha}}{\alpha!} + s^{2\alpha}\frac{\tau_{qh}^{2\alpha}}{(2\alpha)!}\right]\nabla^2\theta^* = \left[s + s^{\alpha+1}\frac{\tau_{Th}^{\alpha}}{\alpha!} + s^{2\alpha+1}\frac{\tau_{Th}^{2\alpha}}{(2\alpha)!}\right](\vartheta^* - \eta_c\lambda_c\psi^*) \tag{36}$$

$$\left[1 + s^{\beta}\frac{\tau_{qm}^{\beta}}{\beta!} + s^{2\beta}\frac{\tau_{qm}^{2\beta}}{(2\beta)!}\right]\nabla^2\psi^* = \left[s + s^{\beta+1}\frac{\tau_{Cm}^{\beta}}{\beta!} + s^{2\beta+1}\frac{\tau_{Cm}^{2\beta}}{(2\beta)!}\right]\left(\frac{\psi^* - \theta^*}{K}\right) \tag{37}$$

where $\vartheta^* = \vartheta^*(r, s)$ and $\theta^* = \theta^*(r, s)$, – and the asterisk is the transformed function in the Laplace domain.

We introduce a modified finite spherical Hankel integral transform [42] stated as

$$H_{0n}[f(r)] = \overline{f}(\omega_n) = \int_0^1 f(r)\, r^2 j_0(\omega_n r)\mathrm{d}r \tag{38}$$

$$f(r) = \left(\frac{4}{\pi}\right)\sum_{n=1}^{\infty}\frac{\omega_n}{[J'_{1/2}(\omega_n)]^2}\int_0^1 \overline{f}(r)\, j_0(\omega_n r) r^2 \mathrm{d}r \tag{39}$$

and the orthogonal property as

$$H_0\left[\frac{\mathrm{d}^2 f}{\mathrm{d}r^2} + \frac{2}{r}\frac{\mathrm{d}f}{\mathrm{d}r}\right] = -\omega_n^2\,\overline{f}(\omega_n) + \omega_n\, j_0(\omega_n)\; f(\omega_n)|_{r=1} \tag{40}$$

where – the kernel is given as $j_0(\omega_n r) = \sqrt{\pi/(2\omega_n r)}\, J_{1/2}(\omega_n r)$, the eigenvalues ω_n are defined by the solution of $j_0(\omega_n) = 0$, with ω_n is an nth root of the spherical Bessel function $j_0(\omega_n r)$ of order 0, respectively. Here, $[J'_{1/2}(\omega_n)]^2 = 2\int_0^1 [J_{1/2}(\omega_n r)]^2 r\, \mathrm{d}r$ [43] where prime denotes the differentiation of $J_{1/2}(\omega_n r)$.

Applying the transform defined by Eq. (38) to Eqs. (35)–(37) and keeping boundary conditions $\theta^*(1, s) = \wp_\theta(s)$ and $\psi^*(1, s) = \wp_\psi(s)$ in mind, one obtains

$$\overline{\vartheta}^* = 1 - b\,[\omega_n^2\,\overline{\theta}^* + j_0(\omega_n)]\, q_\theta(t) \tag{41}$$

$$\Omega_1(s)[-\omega_n^2\,\overline{\theta}^* + j_0(\omega_n)]\,\wp_\theta(s) = \Gamma_1(s)(\overline{\vartheta}^* - \eta_c\lambda_c\overline{\psi}^*) \tag{42}$$

$$\Omega_2(s)[-\omega_n^2\,\overline{\psi}^* + j_0(\omega_n)]\,\wp_\psi(s) = \Gamma_2(s)(\overline{\psi}^* - \overline{\theta}^*)/K \tag{43}$$

where $\overline{\theta}^* = \overline{\theta}^*(\omega_n, z, s)$, $\overline{\psi}^* = \overline{\psi}^*(\omega_n, z, s)$ is the transformed function of θ^*, ψ^*, and the single overbar (¯) means a function in the transformed domain, respectively. Here.

$$\Omega_1(s) = 1 + s^{\alpha}[\tau_{qh}^{\alpha}/\alpha!\,] + s^{2\alpha}[\tau_{qh}^{2\alpha}/(2\alpha)!\,], \tag{44}$$

$$\Gamma_1(s) = s + s^{\alpha+1}[\tau_{Th}^{\alpha}/\alpha!\,] + s^{2\alpha+1}[\tau_{Th}^{2\alpha}/(2\alpha)!\,], \tag{45}$$

$$\Omega_2(s) = 1 + s^{\beta}[\tau_{qm}^{\beta}/\beta!\,] + s^{2\beta}[\tau_{qm}^{2\beta}/(2\beta)!\,] \tag{46}$$

$$\Gamma_2(s) = s + s^{\beta+1}[\tau_{Cm}^{\beta}/\beta!\,] + s^{2\beta+1}[\tau_{Cm}^{2\beta}/(2\beta)!\,] \tag{47}$$

Eliminating $\overline{\vartheta}^*$ from Eqs. (41) and (42), one gets

$$r^2\omega_n^2[\omega_n^2\,\overline{\theta}^* - \Gamma_1(s)(-1 + \eta_c\lambda_c\overline{\psi}^* + b\wp_\theta(s)\omega_n^2)]^2 = \wp_\theta^2(s)[1 + b\Gamma_1(s)]^2\sin^2(r\omega_n) \tag{48}$$

Solving Eqs. (43) and (48), one obtains

$$\overline{\theta}^* = \frac{\Gamma_1(s)(r\omega_n)^2 A_4 + [-\wp_\psi(s)\Gamma_1(s)A_2 + A_1A_4]\sin(r\omega_n)}{(r\omega_n)^2\{A_2A_3 + [-1 + b\wp_\theta(s)\Gamma_1(s)]\omega_n^2[\Gamma_2(s) + \omega_n^2]\}} \tag{49}$$

$$\overline{\psi}^* = \frac{A_3(r\omega_n)^2 + \{\wp_\psi(s)r[-1 + b\wp_\theta(s)\Gamma_1(s)]\omega_n^3 + A_1\Gamma_2(s)r\omega_n\}\sin(r\omega_n)}{(r\omega_n)^2\{A_2A_3 + [-1 + b\wp_\theta(s)\Gamma_1(s)]\omega_n^2[\Gamma_2(s) + \omega_n^2]\}} \tag{50}$$

where $A_1 = \wp_\theta(s)[1 + b\Gamma_1(s)]$, $A_2 = \eta_c\lambda_c$, $A_3 = \Gamma_1(s)\Gamma_2(s)$, $A_4 = \Gamma_2(s) + \omega_n^2$.

Applying the inversion theorem of finite Hankel transform as given in Eq. (39) on Eqs. (49) and (50), one obtains

$$\theta^* = (4/\pi)\sum_{n=1}^{\infty} B_1\{\Gamma_1(s)(r\omega_n)^2 A_4 + [-\wp_\psi(s)\Gamma_1(s)A_2 + A_1A_4]\sin(r\omega_n)\}j_0(\omega_n r) \tag{51}$$

$$\psi^* = (4/\pi)\sum_{n=1}^{\infty} B_1\{A_3(r\omega_n)^2 + \{\wp_\psi(s)r[-1 + b\wp_\theta(s)\Gamma_1(s)]\omega_n^3 \times A_1\Gamma_2(s)r\omega_n\}\sin(r\omega_n)\}j_0(\omega_n r) \tag{52}$$

The functions presented in Eqs. (51) and (52) describe the general solution of temperature and moisture distribution at every instant and at all places of a solid sphere when sectional hygrothermal loading is applied in generalized form. Therefore, Eqs. (51)–(52) represent the Laplace domain's governing equations.

Substituting Eqs. (51) and (52) in Laplace transformed function $g^* = \theta^* + (\gamma_2/\gamma_1)\lambda_c\psi^*$, one obtains

$$g^* = (4/\pi)\sum_{n=1}^{\infty} B_1\big\langle[\Gamma_1(s)A_4 + \varpi A_3](r\omega_n)^2 - \wp_\psi(s)\Gamma_1(s)A_2 + A_1A_4 + \varpi\sin(r\omega_n)\big\{\wp_\psi(s)r[-1 + bq_\theta(s)\Gamma_1(s)]\omega_n^3 + A_1\Gamma_2(s)r\omega_n\big\}\big\rangle j_0(\omega_n r) \tag{53}$$

where

$$B_1 = \omega_n[J'_{1/2}(\omega_n)]^2/\big\langle(r\omega_n)^2\big\{A_2A_3 + \big[-1 + b\wp_\theta(s)\Gamma_1(s)]\omega_n^2[\Gamma_2(s) + \omega_n^2\big]\big\}\big\rangle,$$
$$\varpi = (\gamma_2/\gamma_1)\lambda_c.$$

3.2 Solution of the hygrothermoelastic field

Using Eqs. (53) and (34) will take the form

$$u_r^* = \frac{4}{\sqrt{2\pi}}\sum_{n=1}^{\infty}(B_1/\omega_n^{1/2})\big\langle[\Gamma_1(s)A_4 + \varpi A_3](r\omega_n)^2 - \wp_\psi(s)\,\Gamma_1(s)A_2 + A_1A_4 + \varpi\sin(r\omega_n)\big\{\wp_\psi(s)r[-1 + b\wp_\theta(s)\Gamma_1(s)]\omega_n^3 + A_1\Gamma_2(s)r\omega_n\big\}\big\rangle \times\left\{\frac{1}{r^2}\int_0^r r^{3/2}J_{1/2}(\omega_n r)\,\mathrm{d}r + \frac{2(1-2\upsilon)}{1+\upsilon}\,r\int_0^1 r^{3/2}\,J_{1/2}(\omega_n r)\,\mathrm{d}r\right\} \tag{54}$$

$$\sigma_{rr}^* = \frac{4}{\sqrt{2\pi}}\sum_{n=1}^{\infty}(B_1/\omega_n^{1/2})\big\langle[\Gamma_1(s)A_4 + \varpi A_3](r\omega_n)^2 - \wp_\psi(s)\Gamma_1(s)A_2 + A_1A_4 + \varpi\sin(r\omega_n)\big\{\wp_\psi(s)r[-1 + b\wp_\theta(s)\Gamma_1(s)]\omega_n^3 + A_1\Gamma_2(s)r\omega_n\big\}\big\rangle \times\left\{2\int_0^1 r^{3/2}J_{1/2}(\omega_n r)\,\mathrm{d}r + \frac{2}{r^3}\int_0^r r^{3/2}J_{1/2}(\omega_n r)\,\mathrm{d}r\right\} \tag{55}$$

$$\sigma^{*}_{\varphi\varphi} = \frac{4}{\sqrt{2\pi}} \sum_{n=1}^{\infty} (B_1/\omega_n^{1/2}) \Big\langle [\Gamma_1(s)A_4 + \varpi A_3](r\omega_n)^2 - \wp_\psi(s)\Gamma_1(s)A_2 + A_1A_4 + \varpi \sin(r\omega_n)\big\{\wp_\psi(s)r[-1 + bq_\theta(s)\Gamma_1(s)]\omega_n^3 + A_1\Gamma_2(s)r\omega_n\big\}\Big\rangle \times \left\{ 2\int_0^1 J_{1/2}(\omega_n r)\, r^{3/2}\mathrm{d}r + \frac{1}{r^3}\int_0^r J_{1/2}(\omega_n r)\, r^{3/2}\mathrm{d}r - \left(\frac{\omega_n}{r}\right)^{1/2} J_{1/2}(\omega_n r) \right\} \tag{56}$$

where

$$\int_0^1 r^{3/2} J_{1/2}(\omega_n r)\,\mathrm{d}r = \sqrt{\frac{2}{\pi}}\frac{1}{\omega_n^{5/2}}[-\omega_n \cos(\omega_n) + \sin(\omega_n)] \tag{57}$$

$$\int_0^r J_{1/2}(\omega_n r)\, r^{3/2}\mathrm{d}r = \sqrt{\frac{2}{\pi}}\frac{1}{\omega_n^{5/2}}[-r\omega_n \cos(r\omega_n) + \sin(r\omega_n)] \tag{58}$$

4 The numerical inversion of the Laplace transforms

Consider the Gaver–Stehfest algorithm [44–46], which aims to approximate $f(t)$ by a sequence of functions, can be given as

$$f(t) \approx f_n(t) = \left[\frac{1}{t}\mathrm{In}(2)\right] \sum_{n=1}^{L} a_n\, F\left[\frac{n}{t}\mathrm{In}(2)\right],\ n \geq 1,\ t > 0, \tag{59}$$

where $F[\,.\,]$ is the Laplace transform of $f(t)$.

The coefficients a_n depend only on the number of expansion terms n, defined as

$$a_n = (-1)^{n+L/2} \sum_{k=[(n+1)/2]}^{\min(n,L/2)} \frac{k^{L/2}(2k)!}{(L/2-k)!\,k!\,(k-1)!\,(n-k)!\,(2k-n)!},\ n \geq 1,\ 1 \leq L \leq n \tag{60}$$

Here, the convergence of the Gaver–Stehfest algorithm for numerical inversion of the Laplace transform was established by Kuznetsov [47]. It is well proved that the approximations $f_n(t)$ converge to $f(t)$ if f is continuous at t and of bounded variation in a neighborhood of t.

5 Numerical results, discussion, and remarks

In this section, we focus on illustrating an example demonstrating the impact of temperature and moisture response on the transient hygrothermal stresses in a centrally symmetric solid sphere with a radius 0.2 m subjected to heat and moisture flux. For this purpose, in numerical calculations, we chose a fiber-reinforced composite sphere prepared from Thornel (Union Carbide) T300 graphite fibers and Narmco 5208 epoxy resin [1]. The 1:1 quasi-isotropic hybrid consists of four glass plies oriented at a + 45° angle and two transitional zones where glass and graphite or vice versa. The proportion of graphite with a 0° orientation to graphite with a 90° orientation is equal, resulting in a true interleaving structure. It is observed that even energetic radiation does not significantly alter material moisture absorption characteristics, tensile strength, or buckling modulus. However, saturated steam exposure causes cracking and material loss due to significant changes in moisture absorption. The graphite fiber-reinforced epoxy matrix composite (T300/5208) was chosen for numerical calculations with the following material properties: $\gamma_1 = 31.3 \times 10^{-6}$ cm/cm × K, $\gamma_2 = 2.68 \times 10^{-3}$ cm/cm × K wt% H_2O, $\upsilon = 0.33$, $L = 6.90 \times 10^{-6}\,\mathrm{cm}^2/\mathrm{hr}$, $D = 6.90 \times 10^{-7}\mathrm{cm}^2/\mathrm{hr}$. The physical parameters as $\eta_c = 0.122$ kg/m^{3}K, $\lambda_c = 2.053\,\mathrm{m}^3\mathrm{K/kg}$, and the fractional order $\alpha = 0.2, 0.4, 0.6, 0.8$, $\beta = 0.6$ is taken as a special case. The prescribed sectional temperature and moisture supply is taken as $\theta(1, t) = \delta(t)$ and $\psi(1, t) = \delta(t)$, $\delta(t)$ is the well-known Dirac delta function.

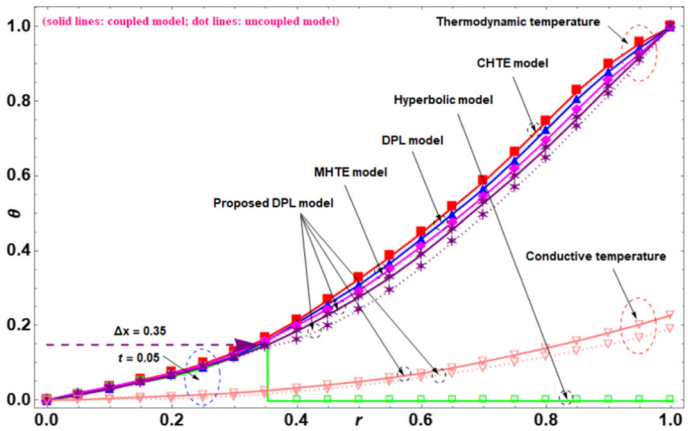

Fig. 2 Comparisons between models (solid: coupled; dash: uncoupled)

Table 1 Temperature θ variation amid different hygrothermoelastic models

r	CHTE	Hyperbolic	DPL	MHTE	Proposed DPL
0	0	0	0	0	0
0.1	0.0341	0.0345	0.0331	0.0354	0.0290
0.2	0.0728	0.0661	0.0695	0.0715	0.0659
0.3	0.1273	0.1188	0.1169	0.1236	0.1140
0.4	0.2134	0	0.2066	0.2004	0.1849
0.5	0.3254	0	0.3093	0.2944	0.2761
0.6	0.4485	0	0.4327	0.4129	0.3901
0.7	0.5852	0	0.5661	0.5461	0.5281
0.8	0.7456	0	0.7248	0.6965	0.6741
0.9	0.8979	0	0.8801	0.8586	0.8389
1	1	0	1	1	1

5.1 Validation of the proposed model with existing model

In order to validate the precision of the current model, it is compared with different model approaches. The comparative analysis is depicted in Fig. 2. In the context of this discussion, the term "solid" refers to a state of being coupled, whereas the "dash" refers to uncoupled, that is, $\eta_c = \lambda_c = 0$. Following [48, 49], the heat propagation velocity can be obtained as $V = \{1/[\tau_{Th}^1 D_C^1 + (1/2)\tau_{Th}^2 D_C^2]\}^{1/2}$ from Eq. (24), where the fractional derivative [50, 51] is taken as $D_C^\alpha f(t) = [1/\Gamma(n-\alpha)] \int_0^t (t-\tau)^{n-\alpha-1} [d^n f(\tau)/d\tau^n)]\, d\tau$, $n-1 < \alpha < n$. Taking $\tau_{Th}^1 = 0.04$ and $\tau_{Th}^2 = 0.0016$, one obtains, $V = \sqrt{50}$. The dimensionless propagation distance $\Delta x = Vt = \sqrt{50}\,t = 0.35$ (here $t = 0.05$), is in good agreement with the numerical prediction [49]. The dimensionless hyperbolic temperature increases with the increase in radial position at a distance of less than 0.35. However, the dimensionless temperature is inverse when the dimensionless position is larger than 0.35. The area integral of the temperature distribution along the position denotes the absorption heat from the external heat source, and the temperature distributions of different models at a certain time represent the other heat transfer mechanisms. The above aspects indicate that the derivations presented in the preceding part are accurate, and the numerical method employed demonstrates efficiency, including hygrothermal coupling, which results in a more rapid temperature response than the absence of hygrothermal coupling. The observed phenomenon can be attributed, at least in part, to the propagation of moisture waves resulting from the interaction between heat and moisture.

The results discussed in this section are listed in Table 1, to conduct a comparative influence of Fourier heat conduction and Fick's moisture diffusion derivatives of the various hygrothermal models. The collected results are presented in tabular format, making it easier for other researchers to compare and verify the accuracy of the results.

The proposed non-simple DPL model can be reduced to a parabolic model by taking equal fractional order $\alpha = \beta = 1$ under uniform initial conditions $\tau_{qh} = \tau_{Th} = \tau_{Cm} = \tau_{qm} = 0$, temperature discrepancy factor $b = 0$, and considering two temperatures as $T = \Phi$ in Eqs. (10) and (15), thus leading to the CHTE

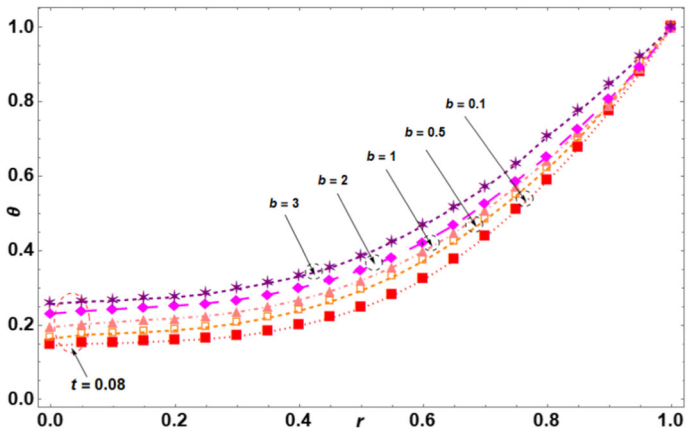

Fig. 3 Coupled temperature profile along r and t for various $b = 0.1, 0.5, 1, 2, 3$

model [38]. The maximum temperature occurs at the outer surface owing to the energy accumulation due to the sectional heat supply, and it drops toward the inner core for both coupled and uncoupled cases; only the magnitude becomes less for uncoupled temperature distribution. The previously cited model aspects support the accuracy of the derivations presented in the preceding part and the efficiency of the mathematical approach employed. Furthermore, when considering hygrothermal coupling, the temperature response exhibits a higher rate of change than without coupling, possibly due to the propagation of moisture waves resulting from the coupling of heat and moisture.

5.2 Effect of temperature discrepancy factor on temperature profile

Figure 3 illustrates the graph depicting the temperature distribution along r for various values of the temperature discrepancy factor b. When the value $b = 0$ indicates, the above model has been reduced to one-temperature theory, whereas if $b \neq 0$ it represents two-temperature theories. Temperature distribution increases with a rise in the difference of temperature value factor b. The maximum temperature occurs at the outer curved surface of the sphere due to the uniform sectional heat supply. When $b = 3$, the temperature graph shows a steep rise due to the energy conversion of heat energy to strain energy. It is learned that the vapor–liquid interface cannot find a stable state at the initial stage irrespective of b value; the temperature and humidity keep a high magnitude. Furthermore, it is worth noting that initially, at low temperatures load, evaporation only makes a small amount of vapor due to the liquid–vapor interface. The amount of vapor exceeds the system's handle for high temperatures, so it sometimes rushes out periodically, and it is more for the high-temperature discrepancy factor. The obtained outcome is consistent with the findings reported earlier [52].

5.3 Effect of fractional distribution response along time

Based on the constitutive Eqs. (24)–(25), it can be observed that when the fractional moisture rate ($\partial^{\beta}\psi/\partial t^{\beta} > 0$) and ($\partial^{2\beta}\psi/\partial t^{2\beta} > 0$) is positive, moisture functions as a heat source in the context of temperature distribution. On the contrary, when the fractional moisture rate is negative ($\partial^{\beta}\psi/\partial t^{\beta} < 0$) and ($\partial^{2\beta}\psi/\partial t^{2\beta} < 0$), it functions as a heat sink. Similarly, the moisture fields are influenced by the fractional temperature rate ($\partial^{\alpha}\theta/\partial t^{\alpha} > 0$) and ($\partial^{2\alpha}\theta/\partial t^{2\alpha} > 0$), comparably, performance as either a source or sink of moisture depending on its sign. The conclusions drawn are consistent with the inference made in the previous research [39]. Considering Figs. 4 through 8, we will discuss the temperature and moisture distribution in dimensionless for the coupled and uncoupled models along the dimensionless time. For clear understanding, we draw solid lines for the coupled model, and dash lines are used for the uncoupled model; the purple color curve indicates the curve at the lower value of fractional order ($\alpha = 0.2$), followed by Magenta curves at the mid-part has the fractional value ($\alpha = 0.4$), red color indicates the curve at the higher value fractional parameter ($\alpha = 0.9$), and the blue color for conductive temperature.

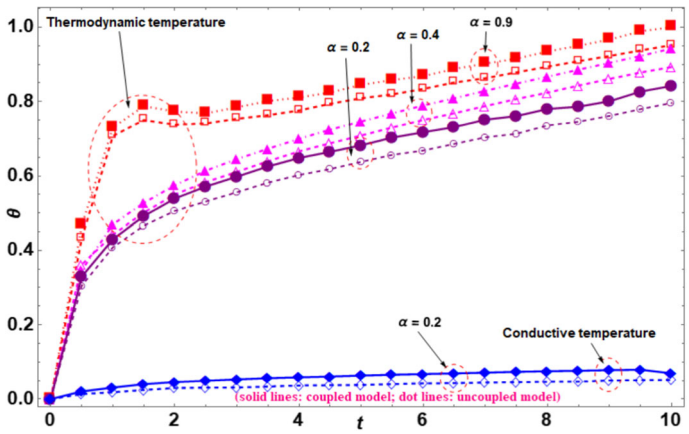

Fig. 4 Temperature profile along t for $b = 1.2, r = 0.8,\ \beta = 0.6$ for different α

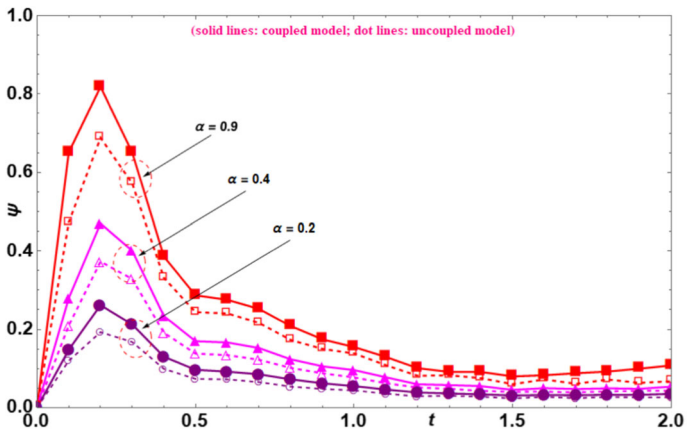

Fig. 5 Moisture profile along t for $b = 1.2, r = 0.8,\ \beta = 0.6$ for different α

Figure 4 illustrates the variation in temperature along dimensionless time t for various fractional-order parameter values α with a fixed value β, and temperature discrepancy factor b. It is learned that both thermodynamic and conductive temperature distribution start increasing with positive values for $0 < t < 1.4$ and then slightly gain stability from $t > 1.4$ for all the phase lags under consideration. As expected, the temperature increases with time toward its sphere's periphery, reaching its maximum value. The reported results are comparable to those found for the thermodynamic temperature [39, 53], which were derived from physically equivalent assumptions. This phenomenon may be attributed to the presence of a heat supply, which leads to a fast moisture reaction in the vicinity of the surface. Consequently, the moisture field is directly dependent on the ratio of temperature change. If the hygrothermal coupling is disregarded, it becomes apparent that there will be no moisture on the surface, as previously anticipated, due to the absence of moisture supply. According to the hygrothermal coupling theory, it is postulated that temperature changes play a pivotal role in the transportation of moisture within a given environment. It has been observed that when one approaches the heated zone in the sphere, there is a gradual increase in both temperature and moisture levels, as illustrated in both Figs. 4 and 5. The moisture distribution ψ starts increasing with positive values for $0 < t < 0.15$ and decreases gradually from $0.15 < t < 2$ for all the phase lags under consideration, as shown in Fig. 5. Under conditions of low moisture load, evaporation yields a relatively low quantity of vapor, causing the liquid–vapor interface to oscillate at an initial stage, and in a later stage, the mass flow rate gets stabilized.

It is observed that the initial value of displacement at the quiescent state is zero. Subsequently, it exhibits a linear progression until reaching time $t = 0.2$ with increase in fractional order. Following this point, the displacement remains constant for an extended duration, as depicted in Fig. 6. The likely explanation for this phenomenon can be associated with the short time within which the sectional heat energy propagates, preventing its reach to the vicinity of the outer surface and resulting in minimal elastic deformation.

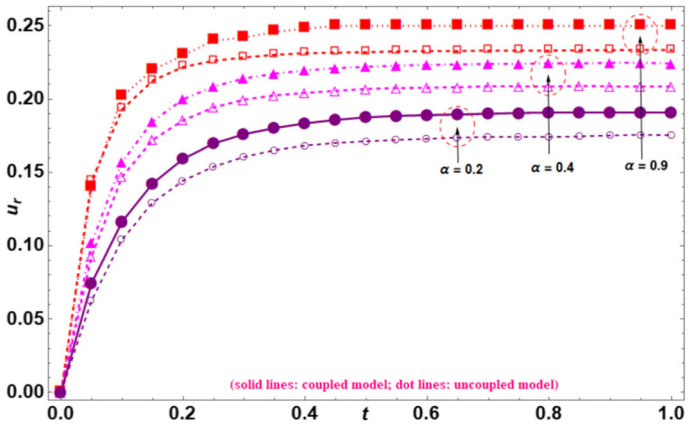

Fig. 6 Displacement along t for $b = 1.2, r = 0.8,\ \beta = 0.6$ for different α

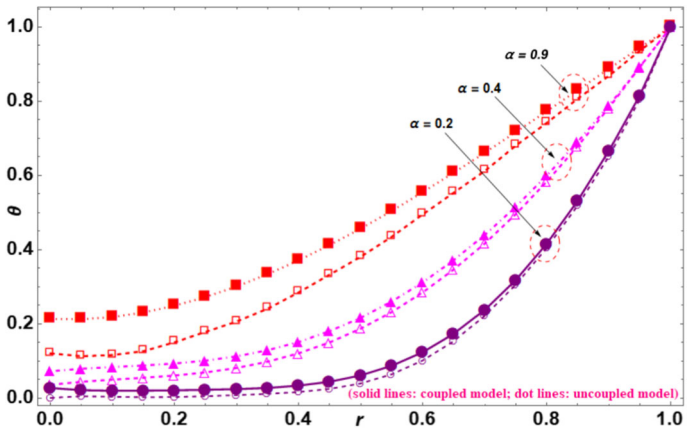

Fig. 7 Temperature profile along r for $b = 1.2, t = 0.8,\ \beta = 0.6$ for different α

5.4 Effect of fractional distribution response along the radius

The dimensionless temperature distribution is smaller at the inner core compared to the outer boundary surface, as shown in Fig. 7. More precisely, the result indicates that temperature is directly proportional to the fractional order for positive values of phase-lag difference. Figure 8 represents the moisture distribution along the radial direction for different fractional orders $\alpha = 0.2, 0.4, 0.9$ and for fixed value $\beta = 0.6$. The moisture distribution ψ gradually decreases as we move toward the outer spherical boundary surface at $r = 1$. Figure 9 shows the nature of radial displacement $u_r(r, t)$ curves, which display similar trends irrespective of changes in fractional orders α and phase-lag variations under consideration. It has been found that the radial displacement is directly proportional to the fractional order α. Therefore, the radial displacement decreases more while approaching classical theory. Later, approximately close to spherical boundary surfaces, and due to the accumulation of sectional heat flux, the displacement curves gain their magnitude to the highest value.

It can be noticed that the radial stress function is found to be compressive at origin and outer curved surface of solid sphere, as depicted in Fig. 10. Investigation shows that the radial stress is directly proportional to the fractional order α along the radial direction for $b = 1.2,\ t = 0.8,\ \beta = 0.6$. The radial stress is zero at the origin as well as the traction-free spherical boundary condition at $r = 1$, as shown in Fig. 11. The radial stress increases instantly for the range $0 < r < 0.06$ due to high tensile force and then decreases substantially. The compressive force is maximum around the outer spherical boundary surface at $r = 1$.

Figure 11 depicts the dimensionless tangential stress $\sigma_{\theta\theta}$ in a solid sphere along the radial direction for various fractional-order parameter values. It can be seen from the figure that the tangential stress along the radial direction increases in a monotonous way from negative to positive values throughout the curve. An increase in the rate of heat propagation may be the cause of the rise in stress. It may be due to heat propagation

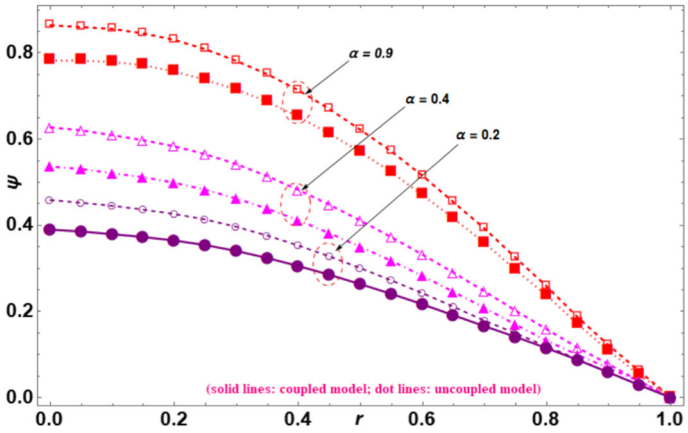

Fig. 8 Moisture profile along r for $b = 1.2, t = 0.8,\ \beta = 0.6$ for different α

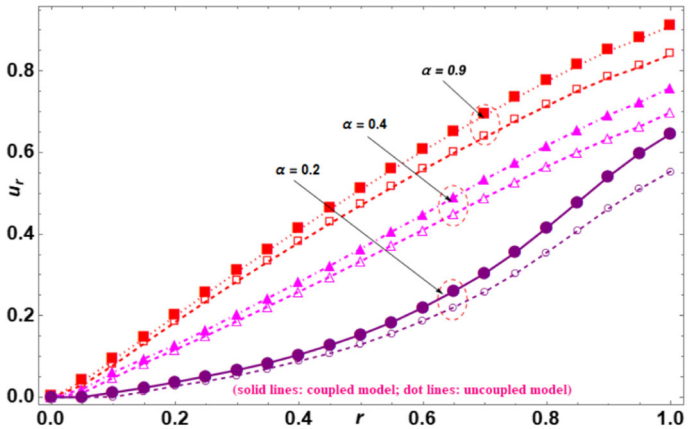

Fig. 9 Displacement profile along r for $b = 1.2, t = 0.8,\ \beta = 0.6$ for different α

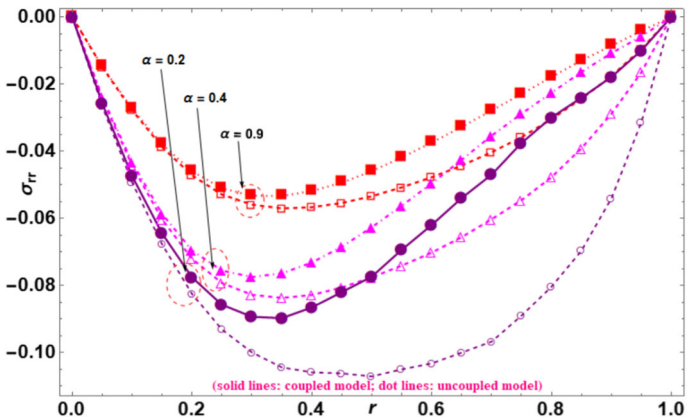

Fig. 10 Radial stress along r for $b = 1.2, t = 0.8,\ \beta = 0.6$ for different α

first resulting in compressive force and then expanding further as the radius approaches closer to the object's surface.

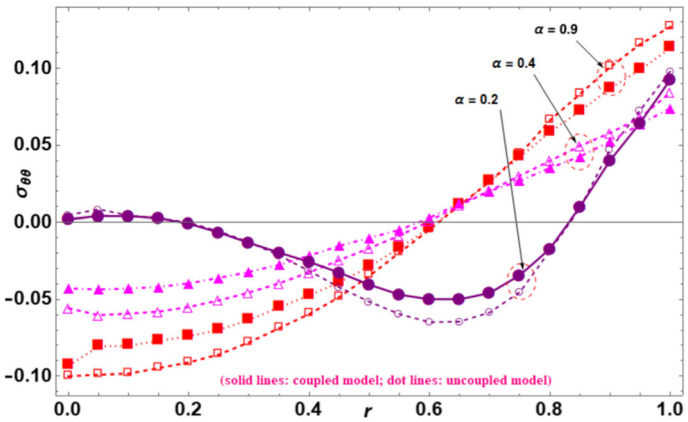

Fig. 11 Tangential stress along r for $b = 1.2, t = 0.8,\ \beta = 0.6$ for different α

6 Conclusion

The proposed study examines a hygrothermoelastic problem involving a centrally symmetric sphere. The investigation is conducted within the context of time-fractional calculus theory. The solid sphere is subjected to physical heat and moisture flux at its outer surface. Introducing the phase-lags parameter into the classical Fourier's and Fick's laws proposes a dual-phase-lag model to study the hygrothermoelastic response under a fractional-order framework. A modified integral technique was employed to derive closed-form solutions for the hygrothermal distribution, displacement, and stress components under unit impulse function. In particular, all the results are compared with those based on the parabolic and hyperbolic hygrothermal coupled models, which were taken as a special case of the present model. Pictographic illustrations have been generated to depict the numerical outcomes relevant to the transient hygrothermoelastic phenomena. The numerical results yield several inferences:

- A new metric evaluates materials' ability to facilitate heat and moisture conduction, considering hygrothermoelastic properties, which can cause temperature decrease without heat transfer to the environment.
- The proposed revised categorization system for materials based on their fractional parameter, following the theoretical framework of hygrothermoelasticity with two temperatures, is necessary. This parameter is a new metric for assessing materials' ability to facilitate heat and moisture conduction, considering the impact of hygrothermoelastic properties.
- The phase lag of the heat and moisture flux and the phase lag of temperature and moisture gradient significantly influence the hygrothermal field variables.
- The theories of coupled classical hygrothermoelasticity, generalized hygrothermoelasticity with two relaxation time, and non-simple dual-phase-lag hygrothermoelasticity can be derived as specific instances.
- The proposed revised categorization system for materials based on their fractional parameter, following the theoretical framework of hygrothermoelasticity with two temperatures, is necessary.

Hence, the findings, as mentioned in the proposed research, have the potential to offer valuable insights for enhancing the heat and moisture management of composites within the context of a fractional-order framework.

Author contributions Shahala Sheikh, Lalsingh Khalsa, Gulshan Makkad, Vinod Varghese wrote the main manuscript and prepared all figures. All authors reviewed the manuscript.

Declarations

Competing interests The authors declare no competing interests.

References

1. Sih, G., Michopoulos, J., Chou, S.C.: Hygrothermoelasticity. Martinus Niijhoof Publishing, Dordrecht (1986)

2. Chang, W.J.: Transient hygrothermal responses in a solid cylinder by linear theory of coupled heat and moisture. Appl. Math. Modell. **18**(8), 467–473 (1994)
3. Benkhedda, A., Tounsi, A., Addabedia, E.A.: Effect of temperature and humidity on transient hygrothermal stresses during moisture desorption in laminated composite plates. Compos. Struct. **82**(4), 629–635 (2008)
4. Zenkour, A.: Hygrothermoelastic responses of inhomogeneous piezoelectric and exponentially graded cylinders. Int. J. Press. Vessels Pip. **119**, 8–18 (2014)
5. Chiba, R., Sugano, Y.: Transient hygrothermoelastic analysis of layered plates with one-dimensional temperature and moisture variations through the thickness. Compos. Struct. **93**(9), 2260–2268 (2011)
6. Ishihara, M., Ootao, Y., Kameo, Y.: Hygrothermal field considering nonlinear coupling between heat and binary moisture diffusion in porous media. J. Therm. Stresses **37**(10), 1173–1200 (2014)
7. Mitra, K., Kumar, S., Vedevarz, A., Moallemi, M.K.: Experimental evidence of hyperbolic heat conduction in processed meat. ASME J. Heat Transf. **117**(3), 568–573 (1995)
8. Tzou, D.Y.: Experimental support for the lagging behaviour in heat propagation. J. Thermophys. Heat Transf. **9**(4), 686–693 (1995)
9. Hetnarski, R.B., Ignaczak, J.: Generalized thermoelasticity. J. Therm. Stresses **22**(4–5), 451–476 (1999)
10. Lord, H.W., Shulman, Y.: A generalized dynamical theory of thermoelasticity. J. Mech. Phys. Solids **15**(5), 299–309 (1967)
11. Green, A., Lindsay, K.: Thermoelasticity. J. Elast. **2**(1), 1–7 (1972)
12. Hetnarski, R.B., Ignaczak, J.: Soliton-like waves in a low temperature nonlinear thermoelastic solid. Int. J. Eng. Sci. **34**(15), 1767–1787 (1996)
13. Green, A., Naghdi, P.: Thermoelasticity without energy dissipation. J. Elast. **31**(3), 189–208 (1993)
14. Tzou, D.Y.: A unified field approach for heat conduction from macro- to micro-scales. ASME J. Heat Transf. **117**(1), 8–16 (1995). https://doi.org/10.1115/1.2822329
15. Chandrasekharaiah, D.: Hyperbolic thermoelasticity: a review of recent literature. Appl. Mech. Rev. **51**(12), 705–730 (1998)
16. Metzler, R., Klafter, J.: The random walk's guide to anomalous diffusion: a fractional dynamics approach. Phys. Rep. **339**(1), 1–77 (2000)
17. Kimmich, R.: Strange kinetics, porous media, and NMR. Chem. Phys. **284**(1–2), 253–285 (2002)
18. Fujita, Y.: Integrodifferential equation which interpolates the heat equation and the wave equation. Osaka J. Math. **27**(2), 309–321 (1990)
19. Luchko, Y., Mainardi, F., Povstenko, Y.: Propagation speed of the maximum of the fundamental solution to the fractional diffusion-wave equation. Comput. Math. Appl. **66**(5), 774–784 (2013)
20. Chaves, A.: A fractional diffusion equation to describe Lévy flight. Phys. Lett. A **239**(1–2), 13–16 (1998)
21. Zanette, D.H.: Macroscopic current in fractional anomalous diffusion. Phys. A **252**(1–2), 159–164 (1998)
22. Gorenflo, R., Mainardi, F., Moretti, D., Paradisi, P.: Time fractional diffusion: a discrete random walk approach. Nonlinear Dyn. **29**(1), 129–143 (2002)
23. Povstenko, Y.: Central symmetric solution to the Neumann problem for a time-fractional diffusion-wave equation in a sphere. Nonlinear Anal. Real World Appl. **13**(3), 1229–1238 (2012)
24. Povstenko, Y.: Fractional heat conduction equation and associated thermal stress. J. Therm. Stresses **28**(1), 83–102 (2004)
25. Sherief, H.H., El-Sayed, A., El-Latief, A.A.: Fractional order theory of thermoelasticity. Int. J. Solids Struct. **47**(2), 269–275 (2010)
26. Youssef, H.M.: Theory of fractional order generalized thermoelasticity. ASME J. Heat Transf. **132**(6), 061301 (2010)
27. Ezzat, M.A., El Karamany, A.S.: Theory of fractional order in electro-thermoelasticity. Eur. J. Mech. A. Solids **30**(4), 491–500 (2011)
28. Jumarie, G.: Derivation and solutions of some fractional Black-Scholes equations in coarse-grained space and time—application to Merton's optimal portfolio. Comput. Math. Appl. **59**(3), 1142–1164 (2010)
29. Povstenko, Y.: Time-fractional thermoelasticity problem for a sphere subjected to the heat flux. Appl. Math. Comput. **257**, 327–334 (2015)
30. Andarwa, S., Tabrizi, H.B.: Non-Fourier effect in the presence of coupled heat and moisture transfer. Int. J. Heat Mass Transfer **53**(15–16), 3080–3087 (2010)
31. Silva, F.R., Gonçalves, G., Lenzi, M.K., Lenzi, E.K.: An extension of the linear Luikov system equations of heat and mass transfer. Int. J. Heat Mass Transfer **63**, 233–238 (2013)
32. Zhang, X.Y., Li, X.F.: Transient response of a hygrothermoelastic cylinder based on fractional diffusion wave theory. J. Therm. Stresses **40**(12), 1575–1594 (2017)
33. Peng, Y., Zhang, X.Y., Xie, Y.J., Li, X.F.: Transient hygrothermoelastic response in a cylinder considering non-Fourier hyperbolic heat-moisture coupling. Int. J. Heat Mass Transfer **126**, 1094–1103 (2018)
34. Hartranft, R.J., Sih, G.C.: The influence of the Soret and Dufour effects on the diffusion of heat and moisture in solids. Int. J. Eng. Sci. **18**, 1375–1383 (1980). https://doi.org/10.1016/0020-7225(80)90094-4
35. Ignaczak, J., Ostoja-Starzewski, M.: Thermoelasticity with finite wave speeds. Oxford University Press, Oxford (2010). https://doi.org/10.1093/acprof:oso/9780199541645.001.0001
36. Quintanilla, R.: A well-posed problem for the dual-phase-lag heat conduction. J. Therm. Stress **31**(3), 260–269 (2008). https://doi.org/10.1080/01495730701738272
37. Chen, P.J., Gurtin, M.E.: On a theory of heat conduction involving two temperatures. Z. Angew. Math. Phys. **19**, 559–577 (1968). https://doi.org/10.1007/BF01594969
38. Sugano, Y., Chuuman, Y.: Analytic solution of transient hygrothermoelastic problem due to coupled heat and moisture diffusion in a hollow circular cylinder. Trans. Jpn Soc. Mech. Eng. **59**(564), 1956–1963 (1993)
39. Zhang, X.Y., Peng, Y., Li, X.F.: Time-fractional hygrothermoelastic problem for a sphere subjected to heat and moisture flux. J. Heat Transfer **140**(12), 122002 (2018). https://doi.org/10.1115/1.4041419
40. Mukhopadhyay, S., Prasad, R., Kumar, R.: On the theory of two-temperature thermoelasticity with two phase-lags. J. Therm. Stress **34**(4), 352–365 (2011). https://doi.org/10.1080/01495739.2010.550815

41. Noda, N., Hetnarski, R.B., Tanigawa, Y.: Thermal stresses, 2nd edn. Routledge, London (2003). https://doi.org/10.1201/9780203735831
42. Chen, I.I.H.: Modified Fourier-Bessel series and finite spherical Hankel transform. Int. J. Math. Educ. Sci. Technol. **13**(3), 281–283 (1982). https://doi.org/10.1080/0020739820130307
43. Abramowitz, M., Stegun, I.A.: Handbook of mathematical functions, p. 485. National Bureau of Standards, Washington, D. C. (1965)
44. Gaver, D.P.: Observing stochastic processes and approximate transform inversion. Oper. Res. **14**(3), 444–459 (1966). https://doi.org/10.1287/opre.14.3.444
45. Stehfest, H.: Algorithm 368, numerical inversion of Laplace transforms. Comm. Assn. Comp. Mach. **13**(1), 47–49 (1970). https://doi.org/10.1145/361953.361969
46. Stehfest, H.: Remark on algorithm 368: numerical inversion of Laplace transforms. Commun. Assn. Comput. Mach. **13**(10), 624 (1970). https://doi.org/10.1145/355598.362787
47. Kuznetsov, A.: On the convergence of the Gaver–Stehfest algorithm. SIAM J. Num. Anal. **51**(6), 2984–2998 (2013). https://doi.org/10.1137/13091974X
48. Calvo, I., et al.: Fractional generalization of Fick's law: a microscopic approach. Phys. Rev. Lett. **99**(23), 230603 (2007). https://doi.org/10.1103/PhysRevLett.99.230603
49. Xu, G., Wang, J.: Analytical solution of time fractional Cattaneo heat equation for finite slab under pulse heat flux. Appl. Math. Mech. Engl. Ed. **39**, 1465–1476 (2018). https://doi.org/10.1007/s10483-018-2375-8
50. Caputo, M.: Linear models of dissipation whose q is almost frequency independent, part II. Geophys. J. Roy. Astron. Soc. **13**, 529–539 (1967)
51. Caputo, M.: Elasticita e Dissipazione. Zanichelli, Bologna (1969)
52. Zenkour, A.M., Abouelregal, A.E.: Non-simple magneto-thermoelastic solid cylinder with variable thermal conductivity due to harmonically varying heat. Earthq. Struct. **10**(3), 681–697 (2016). https://doi.org/10.12989/eas.2016.10.3.681
53. Benkhedda, A., Tounsi, A., Adda Bedia, E.A.: Effect of temperature and humidity on transient hygrothermal stresses during moisture desorption in laminated composite plates. Compos. Struct. **82**(4), 629–635 (2008). https://doi.org/10.1016/j.compstruct.2007.04.013
54. Cattaneo, C.: Sur uneForme de I'equation de la Chaleur eliminant le paradoxed'une propagation instantanee'. C. R. Acad. Sci. **247**, 431–433 (1958)
55. Vernotte, P.: Les paradoxes de la théorie continue de l'équation de la chaleur. C. R. Acad. Sci. **246**, 3154–3155 (1958)
56. Ezzat, M.A.: Magneto-thermoelasticity with thermoelectric properties and fractional derivative. Heat Transf. Phys. B **406**, 30–35 (2011)
57. Lotfy, K., Hassan, W.: Normal mode method for two-temperature generalized thermoelasticity under thermal shock problem. J. Therm. Stresses **37**(5), 545–560 (2014). https://doi.org/10.1080/01495739.2013.869145
58. Lotfy, K., El-Bary, A.A., Tantawi, R.S.: Effects of variable thermal conductivity of a small semiconductor cavity through the fractional order heat-magneto-photothermal theory. Eur. Phys. J. Plus **134**(6), 280 (2019)
59. Lotfy, K., Elidy, E.S., Tantawi, R.S.: Piezo-photo-thermoelasticity transport process for hyperbolic two-temperature theory of semiconductor material. Int. J. Mod. Phys. C **32**(7), 2150088 (2021)
60. Abo-Dahab, S.M., Lotfy, Kh., Gohaly, A.: Rotation and magnetic field effect on surface waves propagation in an elastic layer lying over a generalized thermoelastic diffusive half-space with imperfect boundary. Math. Probl. Eng. **2015**, 671783 (2015)

Terms and Conditions

Springer Nature journal content, brought to you courtesy of Springer Nature Customer Service Center GmbH (“Springer Nature”).
Springer Nature supports a reasonable amount of sharing of research papers by authors, subscribers and authorised users (“Users”), for small-scale personal, non-commercial use provided that all copyright, trade and service marks and other proprietary notices are maintained. By accessing, sharing, receiving or otherwise using the Springer Nature journal content you agree to these terms of use (“Terms”). For these purposes, Springer Nature considers academic use (by researchers and students) to be non-commercial.
These Terms are supplementary and will apply in addition to any applicable website terms and conditions, a relevant site licence or a personal subscription. These Terms will prevail over any conflict or ambiguity with regards to the relevant terms, a site licence or a personal subscription (to the extent of the conflict or ambiguity only). For Creative Commons-licensed articles, the terms of the Creative Commons license used will apply.
We collect and use personal data to provide access to the Springer Nature journal content. We may also use these personal data internally within ResearchGate and Springer Nature and as agreed share it, in an anonymised way, for purposes of tracking, analysis and reporting. We will not otherwise disclose your personal data outside the ResearchGate or the Springer Nature group of companies unless we have your permission as detailed in the Privacy Policy.
While Users may use the Springer Nature journal content for small scale, personal non-commercial use, it is important to note that Users may not:

1. use such content for the purpose of providing other users with access on a regular or large scale basis or as a means to circumvent access control;
2. use such content where to do so would be considered a criminal or statutory offence in any jurisdiction, or gives rise to civil liability, or is otherwise unlawful;
3. falsely or misleadingly imply or suggest endorsement, approval , sponsorship, or association unless explicitly agreed to by Springer Nature in writing;
4. use bots or other automated methods to access the content or redirect messages
5. override any security feature or exclusionary protocol; or
6. share the content in order to create substitute for Springer Nature products or services or a systematic database of Springer Nature journal content.

In line with the restriction against commercial use, Springer Nature does not permit the creation of a product or service that creates revenue, royalties, rent or income from our content or its inclusion as part of a paid for service or for other commercial gain. Springer Nature journal content cannot be used for inter-library loans and librarians may not upload Springer Nature journal content on a large scale into their, or any other, institutional repository.
These terms of use are reviewed regularly and may be amended at any time. Springer Nature is not obligated to publish any information or content on this website and may remove it or features or functionality at our sole discretion, at any time with or without notice. Springer Nature may revoke this licence to you at any time and remove access to any copies of the Springer Nature journal content which have been saved.
To the fullest extent permitted by law, Springer Nature makes no warranties, representations or guarantees to Users, either express or implied with respect to the Springer nature journal content and all parties disclaim and waive any implied warranties or warranties imposed by law, including merchantability or fitness for any particular purpose.
Please note that these rights do not automatically extend to content, data or other material published by Springer Nature that may be licensed from third parties.
If you would like to use or distribute our Springer Nature journal content to a wider audience or on a regular basis or in any other manner not expressly permitted by these Terms, please contact Springer Nature at

onlineservice@springernature.com